Honors Theses

Honors College

5-2024

Cell Type-Specific Production of Amyloid Precursor Protein During Infection is Dependent on the Strain of Herpes Simplex Virus 1

Mia Elias

THE UNIVERSITY OF SOUTH ALABAMA
PAT CAPPS COVEY COLLEGE OF ALLIED HEALTH PROFESSIONS

**CELL TYPE-SPECIFIC PRODUCTION OF AMYLOID PRECURSOR
PROTEIN DURING INFECTION IS DEPENDENT ON THE STRAIN OF
HERPES SIMPLEX VIRUS 1**

BY

Mia Elias

A Thesis

Submitted to the Honors College of the
University of South Alabama
in partial fulfillment of the
requirements for the degree of

Bachelor of Science
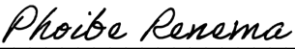
in

Biomedical Sciences

May 2024

Approved: Date:

_____ 05/06/2024
Chair of Thesis Committee: Dr. Robert A. Barrington

_____ 05/06/2024
Committee Member: Dr. Alison Henry

_____ 05/06/2024
Committee Member: Dr. Phoibe Renema

_____ 05/06/2024
Dean of the Honors College: Dr. Douglas A. Marshall

CELL TYPE-SPECIFIC PRODUCTION OF AMYLOID PRECURSOR PROTEIN DURING INFECTION IS DEPENDENT ON THE STRAIN OF HERPES SIMPLEX VIRUS 1

A Thesis

Submitted to the Honors College of the
University of South Alabama
in partial fulfillment of the
requirements for the degree of

Bachelor of Science

in

Biomedical Sciences

by
Mia Elias
May 2024

ACKNOWLEDGEMENTS

I would like to thank my mentor Dr. Robert Barrington for continuously supporting and encouraging my academic achievements throughout my undergraduate career. I would also like to express my gratitude to the members of the Barrington laboratory as this research project would not have been possible without them.

TABLE OF CONTENTS

LIST OF TABLES

LIST OF FIGURES

LIST OF ABBREVIATIONS

α-secretase   Alpha-Secretase

β2M   Beta-2-Microglobulin

γ-secretase   Gamma-Secretase

μL   Microliter

mL   Milliliter

AAALAC   American Association for the Accreditation of Laboratory Animal Care

Aβ   Amyloid Beta

AD   Alzheimer's Disease

ATCC   American Type Culture Collection

APP   Amyloid Precursor Protein

APP KO   Amyloid Precursor Protein Knockout/APP-*deficient*

BACE1   Beta-Secretase

BME   Beta-Mercaptoethanol

BSA   Bovine Serum Albumin

cDNA   Complementary Deoxyribonucleic Acid

Cq   Quantification Cycle

DNA   Deoxyribonucleic Acid

FSC   Forward Scatter

FSC-A	Forward Scatter Area
FSC-H	Forward Scatter Height
GSAP	Gamma Secretase Activating Protein
GEMs	Gel Bead-in Emulsions
GEX	Gene Expression
HSE	Herpes Simplex Encephalitis/Herpetic Encephalitis
HSV-1	Herpes Simplex Virus Type 1
IACUC	Institutional Animal Care and Use Committee
kDa	Kilodalton
MOI	Multiplicity of Infection
NaOH	Sodium Hydroxide
NI	Non-Infected
PBS	Phosphate-Buffered Saline
PI	Propidium Iodide
PSEN-1	Presenilin-1 Protein
RIPA	Radioimmunoprecipitation Assay Buffer
RGE	Relative gene expression
RLT	RNA Lysis Buffer
RNA	Ribonucleic Acid
RT-qPCR	Reverse Transcription Quantitative Polymerase Chain Reaction
sAPPα	Soluble Amyloid Precursor Protein Alpha
sAPPβ	Soluble Amyloid Precursor Protein Beta
scRNA-seq	Single-Cell RNA-Sequence

SSC	Side Scatter
SV40	Simian Vacuolating Virus 40
TBS	Tris-Buffered Saline
TBST	Tris-Buffered Saline with 0.1% Tween® 20 Detergent
TG	Trigeminal Ganglia
WT	Wild-type

ABSTRACT

Mia Elias, B. S., University of South Alabama, May 2024. Cell Type-Specific Production of Amyloid Precursor Protein During Infection is Dependent on the Strain of Herpes Simplex Virus 1. Chair of Committee: Robert A. Barrington, Ph.D.

Cleavage of amyloid precursor protein (APP) generates the antimicrobial peptide amyloid beta (Aβ), the accumulation of which is linked to Alzheimer's Disease (AD) pathogenesis. Whether processing of APP contributes to anti-viral responses is debated. Herpes Simplex Virus Type 1 (HSV-1), a neurotropic double-stranded deoxyribonucleic acid (DNA) virus, establishes lifelong latency and can cause a range of outcomes, from asymptomatic infection to herpetic encephalitis (HSE). Whether disparate outcomes are dependent on HSV-1 strain is unknown. Using three differentially virulent HSV-1 strains, we compared the regulation of APP-associated proteolytic processing in both a corneal infection murine model and an *in vitro* model. By single-cell RNA-sequencing on infected cornea, and by reverse transcription-quantitative polymerase chain reaction (RT-qPCR) on infected corneal fibroblasts, we observed that transcripts of APP, presenilin-1 (PSEN-1), and γ-secretase activating protein (GSAP) were elevated in less neurovirulent strains of HSV-1 relative to the most neurovirulent strain. Furthermore, processing of APP to Aβ was increased in cells infected with less neurovirulent HSV-1. Taken together, these data are consistent with a model whereby APP production and processing shapes neurovirulence of HSV-1.

CHAPTER I

INTRODUCTION

1.1 Background on Alzheimer's Disease

AD is a gradual and progressive neurodegenerative disease caused by neuronal cell death and shrinkage of brain tissue. It is the most common cause of decline in cognitive ability as it accounts for at least two-thirds of cases of dementia in people aged 65 or older and is the sixth leading cause of death in the United States (Kumar *et al.*, 2022). A key hallmark of AD is Aβ plaques in the brain.

1.1.1 Amyloidogenic Pathway

Sequential cleavage of APP generates Aβ, the aggregation of which is linked to the pathogenesis of AD (Kumar *et al.*, 2023). The ɣ-secretase activating protein (GSAP) and presenilin-1 protein (PSEN-1) are critical components in the proteolytic processing of APP into Aβ. In a healthy, typical neuron membrane, two proteases, alpha-secretase (α-secretase) and gamma-secretase (ɣ-secretase), cleave APP to create soluble microscopic peptide fragments outside the cell as shown in **Figure 1**. APP cleavage from α-secretase yields soluble amyloid precursor protein alpha (sAPPα) about 75 kilodaltons (kDa) in size. However, sequential cleavage by β-secretase 1 (BACE-1) and ɣ-secretase results in the formation of APP intracellular domain and Aβ peptides (~40 kDa). The most common isoforms are Aβ1–40, which make up approximately 90% of the resulting

Aβ fragments, and Aβ1–42, which accounts for approximately 10% and is more prone to aggregation (Murphy *et al.*, 2010). Since Aβ1–42 peptides are chemically adhesive, overactivation of the amyloidogenic pathway perpetuates Aβ plaque formation (Cairns *et al.*, 2020). The senile plaques may potentially interfere with and block neuron signaling leading to serious brain function impairment and deterioration as seen in AD (Kumar *et al.*, 2023).

1.1.2 Antimicrobial Properties of Amyloid Beta

The generation of Aβ is theorized to play an important role in the innate immune response to combat microbial infections. This hypothesis suggests that fibrillization of Aβ serves as a mechanism to entrap and neutralize microbes (Whitson *et al.*, 2022).

Novel data suggest that Aβ exhibits antimicrobial activity against various fungal and bacterial infections in mouse and cell culture models of AD (Soscia *et al.,* 2010). Soluble Aβ oligomers bind to microbial cell wall carbohydrates via a heparin-binding domain, inhibiting pathogen adhesion to host cells (Eimer *et al.*, 2018). Aβ oligomers trap bacteria by protofibril-mediated agglutination of unattached microbes (Chu *et al.,* 2012). Once Aβ is bound, microglia engulf the pathogen (Chu *et al.,* 2012; Torrent *et al.,* 2012). Current studies suggest a dual protective and damaging role of Aβ, although these studies are more implicated in bacterial infection (Whitson *et al.,* 2022). There are conflicting reports as to whether the APP pathway is important for anti-viral defenses, specifically in response to HSV-1 infection (Eimer *et al.*, 2018., Bocharova *et al.,* 2021). The work by Eimer and colleagues found that Aβ oligomers inhibit HSV-1 infection *in vitro* and protect 5XFAD mice from acute HSE. In the contrary, using the same approach as Eimer and coauthors, Bocharova and colleagues found that the 5XFAD genotype

failed to protect mice upon infection with two HSV-1 strains (Bocharova *et al.,* 2021; Eimer *et al.*, 2018). Mice that survived HSE cleared HSV-1 infection without triggering extracellular Aβ aggregation in the brain (Bocharova *et al.,* 2021). Therefore, it is unknown if Aβ inhibits HSV-1, an aspect we investigated within this study.

1.2 Herpes Simplex Virus Type-1

HSV-1 is a neurotropic double-stranded DNA virus (Conrady *et al*., 2010) that is mainly transmitted orally, and it causes labial, ocular, and genital infections (Roizman and Zhou, 2015). Over 60% of individuals under 50 years of age are infected with HSV-1 worldwide (Marocci *et al.*, 2020). After primary infection of epithelial cells, the virus establishes latency in sensory neurons of the peripheral ganglia. There are numerous strains of HSV-1: this project focused on strains SC16, RE, and 35. HSV-1 35 is a weakly virulent strain while RE is virulent after corneal infection of mice (Su *et al*., 1990). Unpublished data from our lab demonstrates that strain SC16 (Rajcani *et al.*, 1990) is more lethal than both 35 and RE in mice, indicating that it is highly virulent.

1.2.1 HSV-1 and AD

A growing body of evidence links HSV-1 brain infections to Aβ plaques and to neuronal damage like that found in AD, though direct cause-effect is not established (Marocci *et al.*, 2020). Some of the earliest indications that HSV-1 might be linked to AD were observations in patients with acute HSV-1 infection resulting in HSE that demonstrated similar behavioral characteristics as those with AD (Ball., 1982). Furthermore, studies from the Itzhaki laboratory reported detection of high levels of Herpesviridae DNA from amyloid plaques harvested from postmortem brain tissue of

patients with sporadic AD (Itzhaki, 2017). Even more recently, an epidemiological study in Taiwan reported that those with HSV-1 infection and seropositivity led to a significant risk developing AD, and that antiherpetic treatment at the time of infection markedly reduced that risk by a factor of ten (Cairns *et al.*, 2020). One study that elicited a large interest within AD research, done by Readhead and colleagues, detected an association of HSV infection with AD using a computational strategy which reported greater abundance of HHV6 or HHV7 RNA and DNA in the brains of AD individuals relative to controls (Readhead *et al.*, 2018). This study suggested that herpes viruses drive the production of Aβ peptides. Conversely, separate studies suggest that there is no positive correlation between HSV-1 infection and AD (Jeong and Liu*,* 2019). For example, Jeong and Liu suggest that Redhead *et al.* did not account for extremely low viral RNA and DNA detection limits in their study, leading them to question the positive correlation between HSV-1 infection and AD (Jeong and Liu*,* 2019). Studies from Agostini and Westman examined the correlation between anti-herpes virus antibodies and AD and found that lower titers of anti-Human Herpes Virus-6 IgG correlated with AD (Agostini *et al.*, 2015; Westman *et al.*, 2017). Other data in the field lacks confirmation by other groups, proving causality has remained elusive. In reviewing this literature, only one detailed the strains of HSV-1 examined. Experiments shared herein examine whether different strains of HSV-1 elicit differential production and processing of APP to potentially resolve the controversy in the field.

1.3 Ocular Infection with HSV-1

Corneal infection with HSV-1 is the leading cause of infectious blindness in developed countries (Farooq and Shukla, 2012). There are three routes in which initial corneal HSV-1 infection is thought to enter the brain (Alonso-Vanegas *et al.,* 2016). The first pathway for HSV-1 transmission to the brain is from primary epithelial infection spreading to nearby cells, including fibroblasts, and then via the trigeminal ganglia. The second path involves the reactivation of an initial peripheral infection, utilizing the same neuronal pathways. Additionally, corneal damage has shown to increase with reactivation of HSV-1 due to an immune response (Farooq and Shukla, 2012). Finally, the last mechanism is from the reactivation of latent HSV-1 in the brain. Based on PCR for HSV-1 in the brain, HSV-1 corneal infection can lead to mortality by causing HSE brain in animal models, such as seen in mice (Knotts, FB *et al.,* 1974). Notably, not all strains of HSV-1 can spread to the brain and cause encephalitis indicating that neurovirulence is a key difference between strains (Barrington lab unpublished data; Su *et al.*, 1990; Rajcani *et al.*, 1990). Therefore, strains of HSV-1 that are incapable of reaching the brain in WT mice are less neurovirulent than other strains. For the most neurovirulent strains of HSV-1, corneal infection is an entry point for viral access to the brain. The above observations provide rationale for examining HSV-1 strain-dependent contributions to AD.
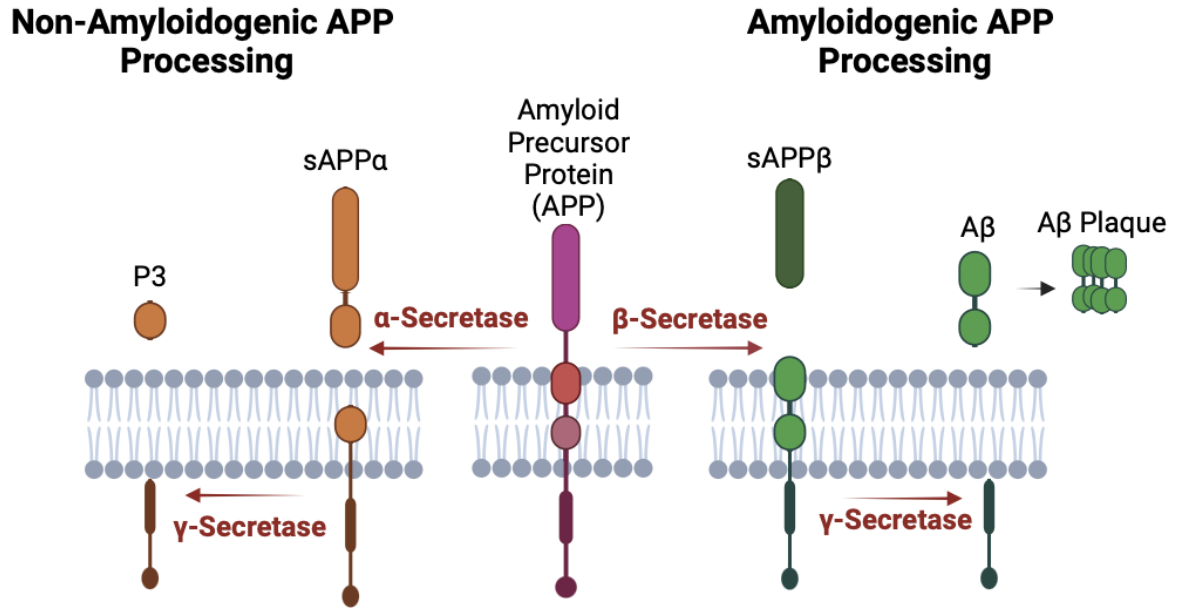
Figure 1. APP Processing Pathways. Non-amyloidogenic (left) and amyloidogenic (right) pathways of APP processing. The γ-Secretase is composed of Presenilin-1 and γ-Secretase Activating Protein. Generated with BioRender.com.

CHAPTER II

HYPOTHESIS AND AIMS

In this study, we hypothesize that HSV-1 induces expression of APP differentially dependent on the neurovirulence of the virus strain. Furthermore, we aim to investigate whether APP is antiviral.

The hypothesis will be addressed with the following aims:

Aim 1. Determine whether APP processing differs in cells infected with three different HSV-1 strains that vary in their neurovirulence.

> Aim 1a: Determine whether genes involved in the processing APP are differentially expressed following intracorneal HSV-1 infection using Single Cell RNA sequencing (scRNAseq).

> Aim 1b: Determine whether APP production and processing differs in corneal fibroblasts infected with HSV-1 SC16, RE, and 35 strains using RT-qPCR and western blot analysis.

Aim 2. Determine whether the production of APP is immunoprotective during HSV-1 infection.

> Aim 2a: Determine whether APP can impair HSV-1 *in vivo* by measuring viral load and corneal pathology in infected wild-type and *APP*-deficient mice (APP KO).

Aim 2b: Determine whether APP inhibits viral infection and/or replication by comparing the amount of virus in WT and APP KO corneal fibroblasts by plaque assay 24 hours after infection.

CHAPTER III

MATERIALS AND METHODS

3.1 Mice

Wild-type (WT) (C57BL/6J; The Jackson Laboratory catalog #000664) and

APP KO mice (B6;12957-APP^{tm1Dbo}/J; The Jackson Laboratory #004133) used for

experiments were housed in an American Association for the Accreditation of Laboratory

Animal Care (AAALAC) at the University of South Alabama College of Medicine. Mice

were euthanized and dissected according to approved protocols by the University of

South Alabama Institutional Animal Care and Use Committee (IACUC).

3.2 Cell Lines

In vitro experiments were conducted using primary murine corneal fibroblasts.

The cells were immortalized by transducing primary fibroblasts with lentivirus encoding

for simian vacuolating virus 40 (SV40) large T antigen by our laboratory.

Vero cells were used for plaque assay as well as propagation of HSV-1. The cells

were purchased from the American Type Culture Collection (ATCC).

3.3 HSV-1 Strains

The Herpes Simplex Virus-1 strains used in this project were 35, RE, and SC16. HSV-1 strains RE and 35 were originally obtained from Ysolina Centifanto-Fitzgerald (Tulane University, New Orleans, La.) and Fred Rapp (Hershey Medical Center, Hershey, Pa.), respectively: Both viruses were propagated as previously described (Su *et al.*, 1990). SC16 was propagated as previously described (Hill *et al.*, 1975). Each of the HSV-1 strains were originally isolated from patients (Metcalf and Michaelis, 1983; Su *et al.*, 1993; Hill *et al.*, 1975). Unpublished data from our lab on mice mortality rates due to corneal infection of HSV-1 was used as a measure of strain virulence. HSV-1 strain SC16 is the most neurovirulent, RE is moderately virulent, and 35 is weakly virulent.

3.4 Generation of Single-Cell RNA-Sequencing Libraries

Mice were infected with 1 x 10^6 plaque forming units per µL of HSV-1 using a 32-gauge Hamilton® needle. 48 hours post-infection, corneas were collected and homogenized using the Miltenyi Biotec gentleMACS^{TM} Tissue. Following homogenization, single-cells were processed through the 10X Genomics workflow: The 10X workflow is shown in **Figure 2**. Single-cell RNA-sequencing (scRNA-seq) libraries were created using 10x Genomics Chromium Next GEM single cell 3' Reagent kit v3.1 with Feature Barcode technology for Cell Surface Protein (10X Genomics., Pleasanton, CA, USA). Libraries were then shipped to Novogene Genomic Services for sequencing. 12 mice were used to generate scRNA-seq libraries of each virally infected mouse condition.

3.4.1 Analysis of scRNA-seq Libraries

Raw single-cell sequencing data were pipelined into Cell Ranger multi for data analysis format. The principal components were set to 10 and the program Loupe GEX was used for data analysis.

3.4.2 Identification of Fibroblast and Epithelial Cell Subsets

Phenotypically differentiable cell populations in the gene expression libraries created (as described in sections 3.6 and 3.6.1) are distinguished by a combination of transcriptional markers. Using markers distinct to each cell subset, we identified and separated putative fibroblast (marker FBN-1) and epithelial cells (marker KRT-12) as established in the literature to be permissive populations to HSV-1 infection (Smiley *et al.,* 1985).

3.4.3 Expression of APP, PSEN-1, and GSAP

After identifying fibroblast and epithelial cell subtypes, the expression levels of APP, PSEN-1, and GSAP were also explored to determine transcriptional differences of APP proteolytic processing components across the conditions.
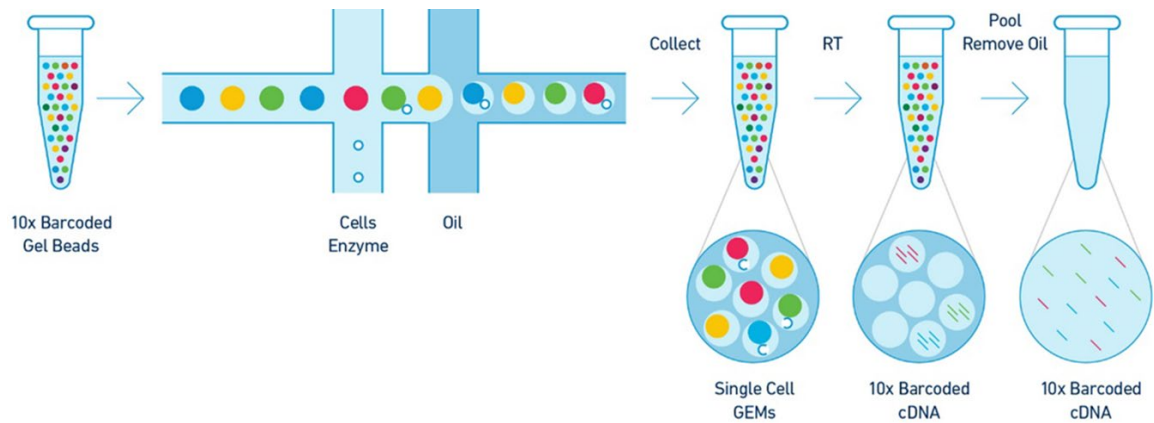
Figure 2. 10X Genomics Processing. Mouse corneas are homogenized and processed through the 10X genomics workflow. 10X Genomics' technology uses gel beads each containing a unique barcode to create Gel Bead-In Emulsions (GEMs). Each of these GEMs contains one cell and one unique barcode. The cell in the GEM is lysed and cDNA is generated via reverse transcription of mRNA. Each cDNA sequence with its unique barcode is sequenced and traced back to the original cell (Figure and caption adapted from 10X Genomics Inc).

3.5 Reverse Transcription Quantitative Polymerase Chain Reaction

Reverse Transcription Quantitative Polymerase Chain Reaction (RT-qPCR) is an experimental method able to quantify specific nucleic acid sequences, allowing assessment of changes in gene expression because of pathology (Sanders *et al.*, 2014). This lab technique was used to measure the impact HSV-1 infection had on APP related gene expression in mouse cells.

Cells (murine corneal fibroblasts) were seeded in cell culture plates. Once the cell monolayer achieved approximately 80-100% confluency, the cells were either left uninfected or infected with one of the three HSV-1 strains (RE, 35, or SC16) at a

multiplicity of infection (MOI) of 30. After 24 hours, the cells were lifted. Ribonucleic

acid (RNA) was isolated from cells using the Qiagen RNeasy Mini Kit. Briefly, cells

were resuspended in 350 μL RNA lysis buffer (RLT) and 10 μL β-Mercaptoethanol

(BME). To remove genomic DNA, cells were spun using a QiaShredder column. RNA

was isolated as per the standard protocol of the Qiagen RNeasy Mini Kit. The RNA was

further converted to complementary DNA (cDNA) by combining 15 μL of the eluate with

1 μL iScript Reverse Transcriptase, and 4 μL iScript Advanced 5x Reaction Mix and

incubated at 25°C for 5 minutes, 42 °C for 30 minutes, and then at 85 °C for 5 minutes.

Stock cDNA was stored at -20 °C. PCR of cDNA was prepared in a 96-well PCR plate,

containing 1 μL of cDNA stock quantified on a spectrophotometer and 19 μL of a master

mix composed of SYBR^{TM} Green (10 μL/well), 10 μM primer designed for a specific

gene (4 μL/well), and nuclease-free water (4 μL/well). The samples were run on a

thermocycler to generate a quantification cycle (Cq) value, indicative of gene expression.

Primers were designed for PSEN-1, GSAP, and a housekeeping gene, β2-micoglobulin

(β2M) as shown in **Table 1.** Both forward and reverse primers were designed using

NCBI Primer-Blast. Each primer was validated by confirming the appropriate size using

gel electrophoresis, as well as ensuring appropriate melt peaks.

Table 1. RT-qPCR Primers for APP Components of Interest.

Gene ID	Primers (5′ → 3′)	Product Size (base pairs)	Validated
β2M*	F: CCCGCCTCACATTGAAATCC R: GCGTATGTATCAGTCTCAGTGG	144	✓
APP	F: TCTGAACTTGGACAGCGAAA R: AAGCCGAGGGTGAGTAAATAAA	106	✓
PSEN-1	F: GGAGGAGAACACATGAGAGAAAG R: GTAGGACAAAGGTGCAGGTATC	106	✓
GSAP	F: GTGCCTAACTTTGCTGGTAGA R: GACTTTCAGCTTGTGGGTAGAG	107	✓

All primers were designed using NCBI Primer-Blast. Housekeeping gene

is denoted with a single asterisk (*). The sequences preceded by "F:" are the forward

primers, while the sequences preceded by "R:" are the reverse primers.

3.6 Western Blot

The western blot is an experimental method that allows for separation and

identification of proteins from various sample types (Mahmood and Yang, 2012).

Protein gel samples consisted of 35.0 μL of supernatants collected 48 hours post-

infection from NI cells and corneal fibroblasts infected with HSV-1 strains SC16, RE,

and 35 at an MOI of 30. Protein gel samples were mixed with 25% BME of the lysate

volume, 16.7% 6X loading dye of the total protein gel sample volume, and

radioimmunoprecipitation assay buffer (RIPA) was added to obtain a final protein gel

sample volume of 100 μL. Samples were heated at 95 °C for 5 minutes and centrifuged.

20 μL per well of each sample was loaded into a Bio Rad Mini-Protein TGX 12% Bis-

Tris Gel, 10-well (reference number 4561044) protein gel with 800 mL 1X NuPage™

MOPS SDS running buffer. Following western transfer at 105 V for 70 minutes to a

nitrocellulose membrane and subsequent 5-minute wash with 1X tris-buffered saline with

0.1% Tween® 20 detergent (TBST), 10 mL Ponceau stain was added to the membrane to

detect protein transference. The Ponceau stain was removed by the addition of 10 mL 5%

sodium hydroxide (NaOH). After a rinse with 1X TBST, the membrane was shaken in 50

mL1X tris buffered saline (TBS) with 5% dry milk for 1 hour to block. The membrane

was cut into necessary strips and then rinsed in 1X TBST 3 times for 5 minutes each. The

primary antibody of choice was diluted with 10 mL 5% bovine serum albumin (BSA) as

shown in **Table 2.** After addition of the primary antibody, the membrane was placed in a

cold room on a shaker overnight. The following day, the primary antibody was removed,

and the membranes were washed 3 times with 5 mL 1X TBST for 10 minutes each.

Following these washes, the proper secondary antibody (Mouse IgG HRP, Southern

Biotech #1032-05) diluted (1:2000) in 1X TBS and 5% dried milk was added to the

membranes. The membranes were subsequently placed in a shaker at room temperature

for 1 hour. Following this incubation period, the secondary antibody was removed, and

the membranes were washed 3 times in 1X TBST. Following these washes, the

membranes were imaged using a ChemiDoc imager on the chemiluminescence setting.

Table 2. Primary Antibodies for Western Blot.

Target	Company	Reference Number	Clone	Host	Dilution
β-Actin	Sigma-Aldrich	A5441	AC-15	Mouse	1:7500
M3.2	BioLegend	8057	M3.2	Mouse	1:2000

3.7 Annexin V/Propidium Iodide Staining

6-well plates which contained 1 x 10^5 corneal fibroblast cells per mL were either left uninfected (negative control) or infected with HSV-1 at a MOI of 30. As a positive control, some non-infected cells were heat-treated to induce cell death. 48 hours post-infection, cells were lifted and centrifuged to remove media. Cells were washed with 3 mL of phosphate-buffered saline (PBS) and centrifuged. BD Pharmingen™ 10X Annexin V Binding Buffer (component no. 51-66121E) was used to make a 1X working solution with distilled water. 85 μL of the 1X working solution was transferred to a 5 mL culture tube; and 5 μL of FITC Annexin V (APC, catalog no. 550475) and 10 μL of Propidium Iodide (PI) (component no. 51-66211E) was added. Cells were gently vortexed and incubated for 30 minutes at 25 °C in the dark. Following incubation, cells were washed with 200 μL 1X working solution, centrifuged, and decanted. 300 μL PBS was added and samples were put through flow cytometry.

3.7.1 Flow Cytometry Analysis

Data from the Agilent NovoCyte® Quanteon™ Flow Cytometer was analyzed using FlowJo™ software (TreeStar., Ashland, OR, USA) as shown in **Figure 3**.
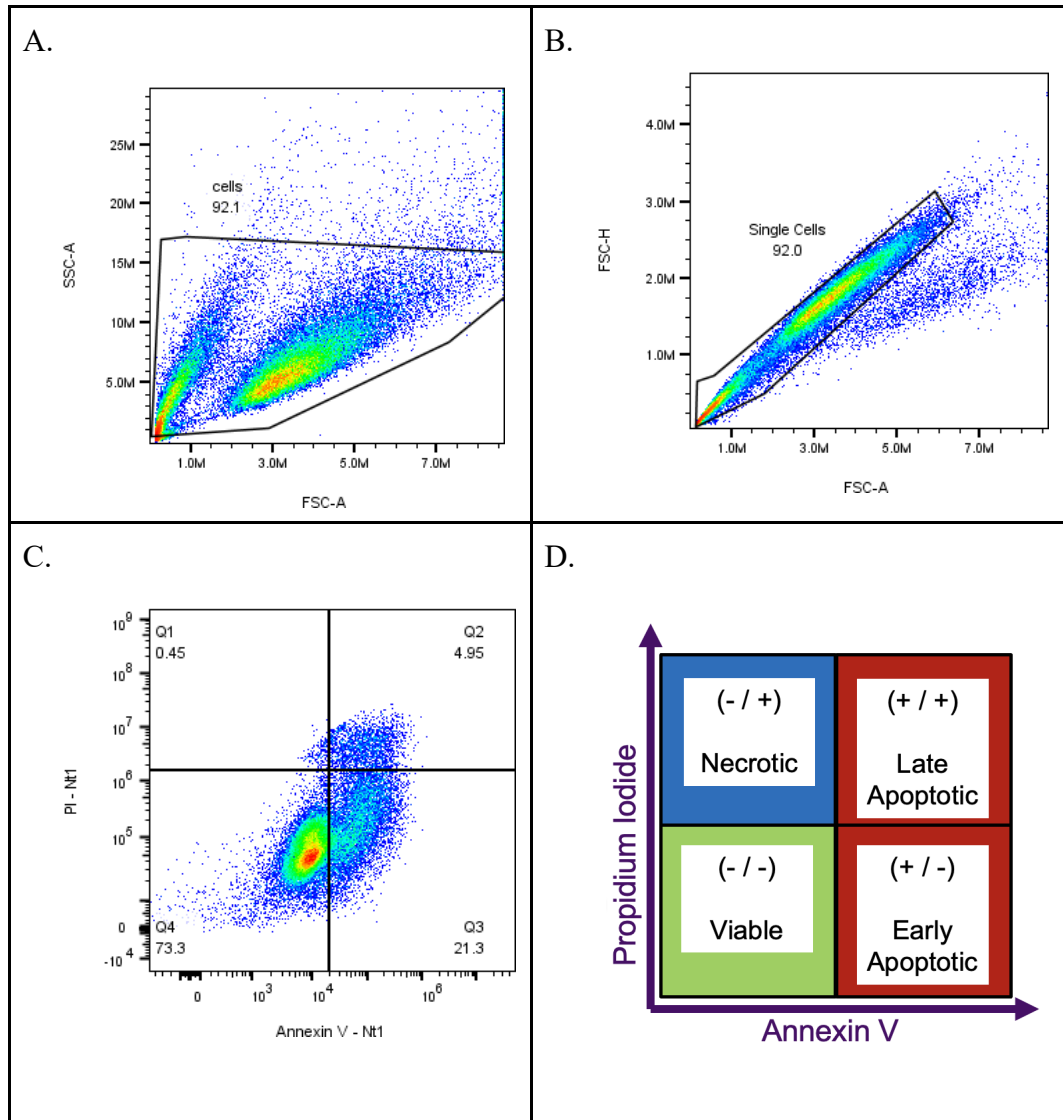
Figure 3. Flow Cytometry Gating Scheme to Identify Viable, Apoptotic, and Necrotic Cells. Flow cytometry separates cells based on size [forward scatter (FSC)], granularity [side scatter (SSC)], and the presence of fluorochromes conjugated to a specific marker or antibody (panel A). Single-cell fibroblasts were identified (panel B) by forward scatter area (FSC-A) and forward scatter height (FSC-H). Necrotic (quadrant 1, -/+), late apoptotic (quadrant 2, +/+), early apoptotic (quadrant 3, +/-), and healthy (quadrant 4, -/-) cells were identified using Annexin V and PI (panels C and D).

3.8 Plaque Assay

A plaque assay was used to determine the viral concentration of HSV-1 SC16, RE, and 35 stocks. 6-well plates were seeded with Vero cells and used when 90-100% confluent. 10-fold serial dilutions were made of the virus stock by taking 100 µL of virus stock and diluting into 900 µL of media, repeating 9 times. 100 µL of -5, -6, -7, -8, and -9 dilutions were added to duplicate wells. Final plaques were counted, and viral titers were calculated as following: 8 plaques on -7 dilution, $8 \times (1 \times 10^7) \times 10$ PFU/mL.

Plaque assay was used to determine viral titer of WT and APP KO corneal fibroblasts infected with HSV-1 SC16, RE, or 35. WT and APP KO CF's were infected with an MOI of 10 of HSV-1 SC16, RE, or 35. A serial 10-fold dilution was prepared using supernatants collected from the cells 24-hours post infection. 100 µL -1, -2, -3, and -4 dilutions was added to duplicate Vero wells.

To determine viral titer of corneas and trigeminal ganglia (TG) infected with HSV-1 RE, WT and APP KO mice were intracorneal infected with 1×10^6 PFU/µL of RE. 48 hours post infection, corneas and TG were collected and homogenized and a 10-fold serial dilution was prepared. Viral titers were analyzed as previously described.

3.9 Intracorneal HSV-1 Infection

The desired dose of HSV-1 infection was injected through an intracorneal route as designed by the Lausch laboratory (Fenton *et al.,* 2002). A 30G disposable needle bevel-up was used to make a pilot hole through the corneal epithelium into the stroma, shown in **Figure 4**. A 32G/30cm needle attached to a repeating dispenser (Hamilton, Reno, NV,

18

USA) was inserted bevel down and 1 μL of HSV-1 was injected into the stroma. 1×10^6

PFU/μL HSV-1 were used for all infections.
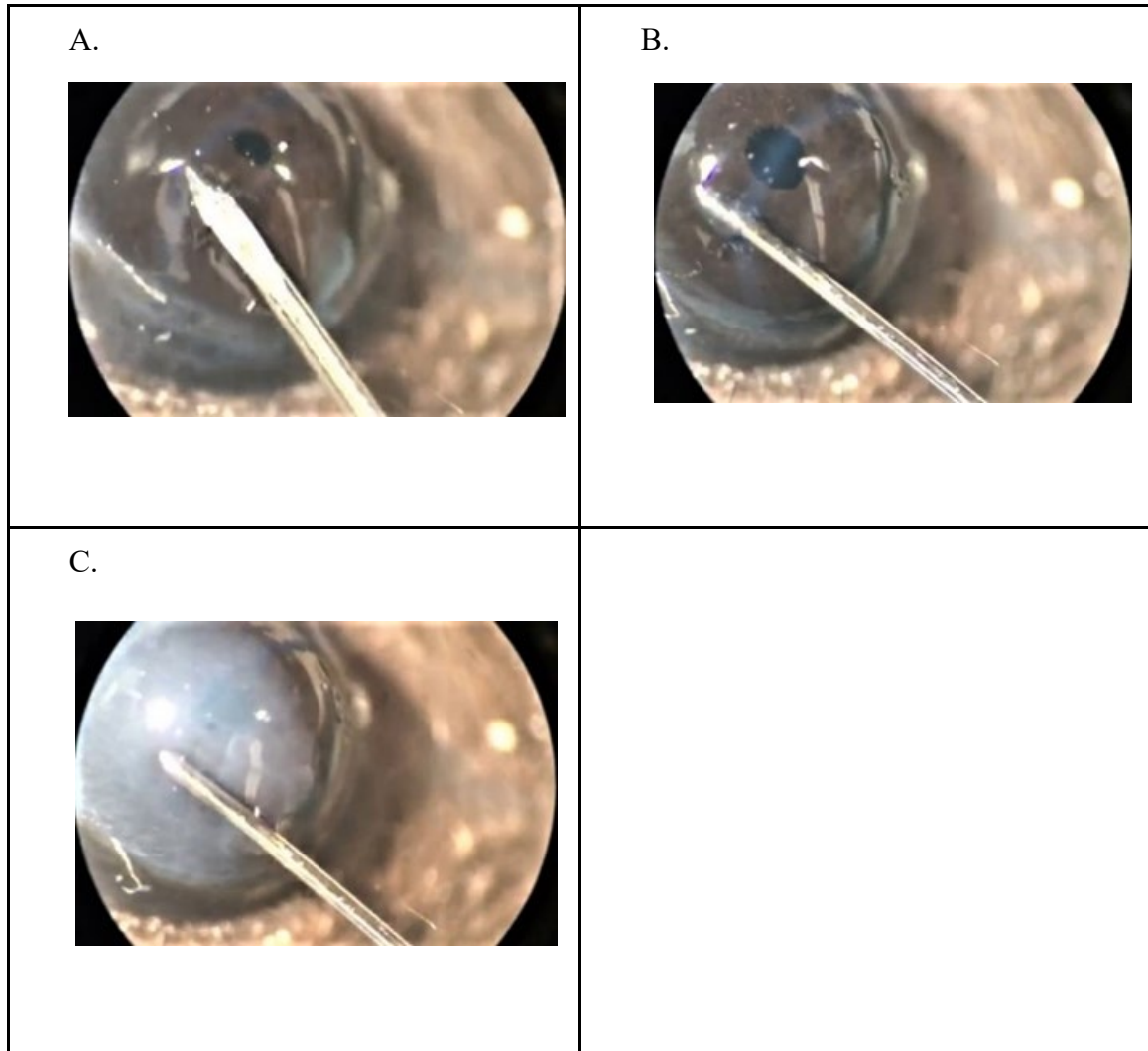
Figure 4. Murine Intracorneal HSV-1 Infection. A) Formation of the pocket for injection. B) Insertion of injection needle. C) Injection of HSV-1 into the cornea. Cloudiness of the cornea indicates a successful injection.

3.10 Scoring Corneal Pathology

Eyes were monitored under a dissecting microscope and scored in a blinded analysis, refer to **Figure 5**. Scores were as follows: 0 = clear, 1 = slight haze, 2 = moderate opacity, 3 = severe opacity, 4 = severe opacity with iris obscured, 5 = necrotizing stromal keratitis.
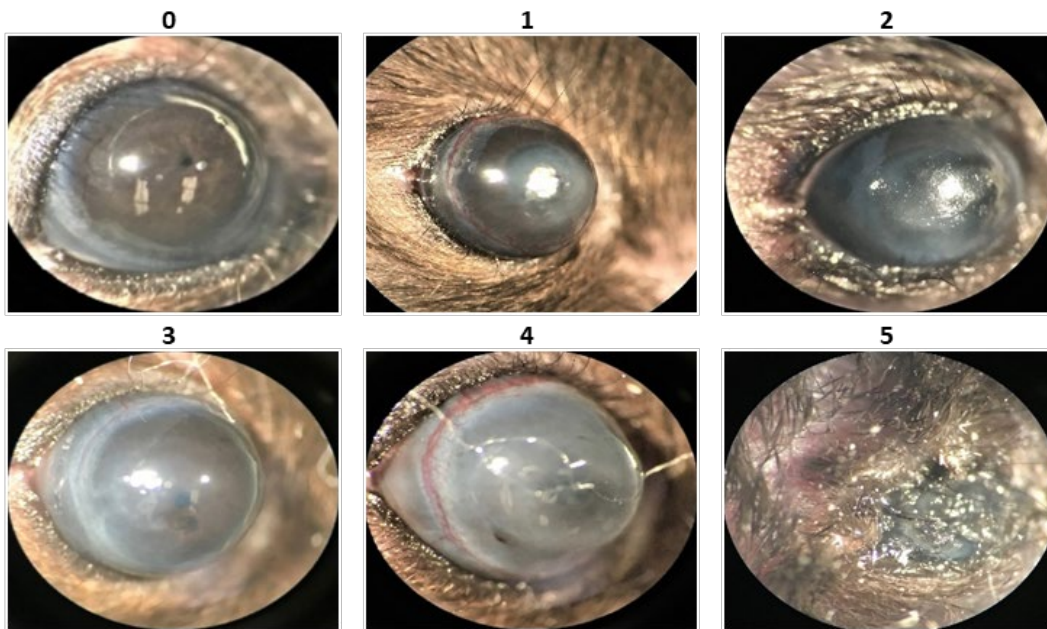
Figure 5. Corneal Pathology Scoring Guide. 0) clear corneas, 1) slight haze, 2) moderate opacity, 3) severe opacity, 4) severe opacity with obscured iris, 5) necrotizing stromal keratitis.

CHAPTER IV

RESULTS

4.1 GEX Library

Fibroblast and epithelial cells expressing APP, PSEN-1, and GSAP in whole mouse cornea infected with HSV-1 SC16, RE, and 35 were identified using the gene expression (GEX) libraries as shown in **Figure 6**. By plotting the frequencies using violin plots as shown in **Figures 7-9,** the relative gene expression was established. Thus, quantification of the transcript indicated the SC16 infected samples had lower transcript levels of APP, PSEN-1, and GSAP in comparison with RE and 35 infected cells. RE and 35 infected cells had similar transcript levels of APP, PSEN-1, and GSAP. Relative gene expression of BACE-1 in NI, whole mouse cornea infected with RE, and infected media (Mock) was plotted using a violin plot as shown in **Figure 10.** Collectively, these transcriptomic data are consistent with our hypothesis that strains of HSV-1 induce APP production and processing differentially.

4.2 Impact of HSV-1 Strain on APP Proteolytic Processing Components

To determine if there were differences in APP, PSEN-1, and GSAP genes following HSV-1 infection in corneal fibroblasts we used RT-qPCR and western blot.

RT-qPCR experiments with cDNA from HSV-1 infected and non-infected fibroblast cells were performed as shown in **Figure 11.** Mean expression of APP, PSEN-1, and GSAP was significantly greater in HSV-1 RE infected cells than both SC16 infected and NI cells. Consistent with the single cell RNAseq data, these results also suggest that expression of APP and processing components are induced differentially dependent on the strain of HSV-1. Of note, APP transcripts varied in HSV-1 35 infection *in vivo* and *in vitro*, revealing potential differences between the two models.

Western blot experiments with supernatants of HSV-1 infected fibroblasts were also performed as shown in **Figure 12.** NI and SC16 infected cells had higher levels of sAPPα (~100 kDa) than processed APP (~45 kDa). Conversely, RE and 35 infected cells had more processed APP than fuller-length APP.

4.3 Number of HSV-1 Infected Cells

We performed a cell death assay using flow cytometry to make inferences on whether the fibroblast cells were infected. The number of viable fibroblast cells, undergoing early apoptosis, late apoptosis, or necrosis was quantified. As shown in **Figure 13**, NI cells were primarily viable (85.6%) and heat-treated cells were primarily undergoing apoptosis (58.1%). There was a substantial increase in viable cells following SC16 infection versus RE (84.5% vs. 11.0%) or 35 (84.5% vs. 16.8%) infection (Figures 10). Inversely, there was a substantial increase in apoptotic cells following RE (88.6% vs. 13.3%) and 35 (82.6% vs. 13.3%) infection versus SC16. There was a small percentage of cells that underwent necrosis in SC16 (1.2%), RE (0.4%), and 35 (0.6%) infected cells. Cell death comparison plots using flow cytometry data are shown in **Figure 14.** Since

corneal fibroblasts were infected using the same plaque forming unit (PFU) of virus, these results suggest that different strains of HSV-1 may vary in their tropism.

<div align="center">

4.4 Corneal Opacity

</div>

To determine the involvement of APP in neutralizing HSV-1 strains, we evaluated corneal pathology. As shown in **Figure 15**, RE infected APP KO mice had increased corneal opacity scores compared to WT mice. Among the mice, the female mouse exhibited the most pronounced opacity in both eyes. These data show APP KO mice are more susceptible to HSV-1 infection suggesting that APP is immunoprotective.

<div align="center">

4.4.1 Viral Titer in WT and APP KO Mice

</div>

RE infected APP KO mice displayed greater corneal viral titer compared to WT mice as shown in **Figure 16**. Viral burden was greatest in the female APP KO mouse. Plaque assay of trigeminal ganglia showed APP KO mice had significantly greater viral load than WT mice, shown in **Figure 17**. These data suggest the APP limits spread and/or replication of HSV-1 to the TG.

<div align="center">

4.4.2 Viral Titer in WT and APP KO Corneal Fibroblasts

</div>

SC16 and RE infected APP KO mice displayed significantly greater viral titer compared to WT mice as shown in **Figure 18** and **Figure 19**, respectively**.** Viral titer in WT and APP KO corneal fibroblasts infected with HSV-1 35 was not different. These data also suggests that APP is immunoprotective *in vitro.*
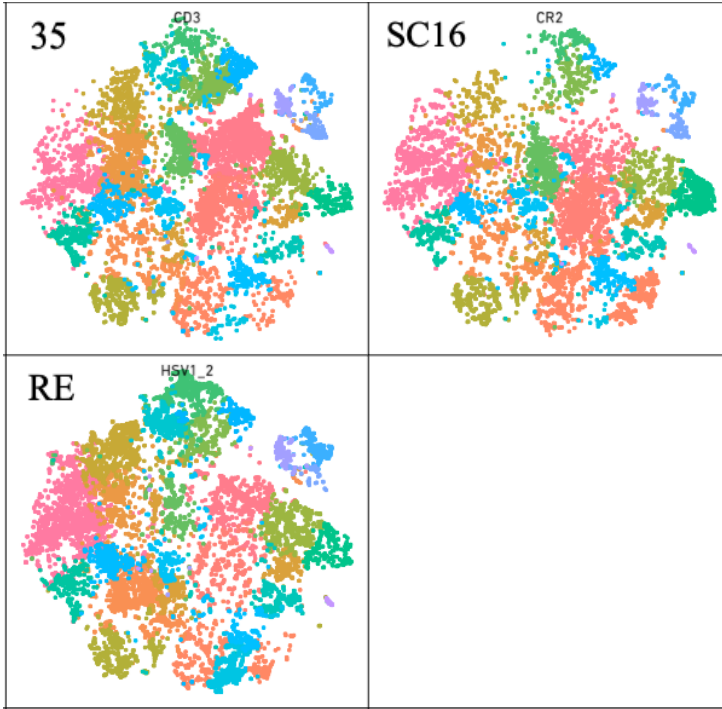
Figure 6. GEX Expression using Loupe GEX Browser. HSV-1 SC16 (top right), 35 (top left), and RE (bottom left) infected murine cornea are grouped in clusters based on similarities in gene expression.
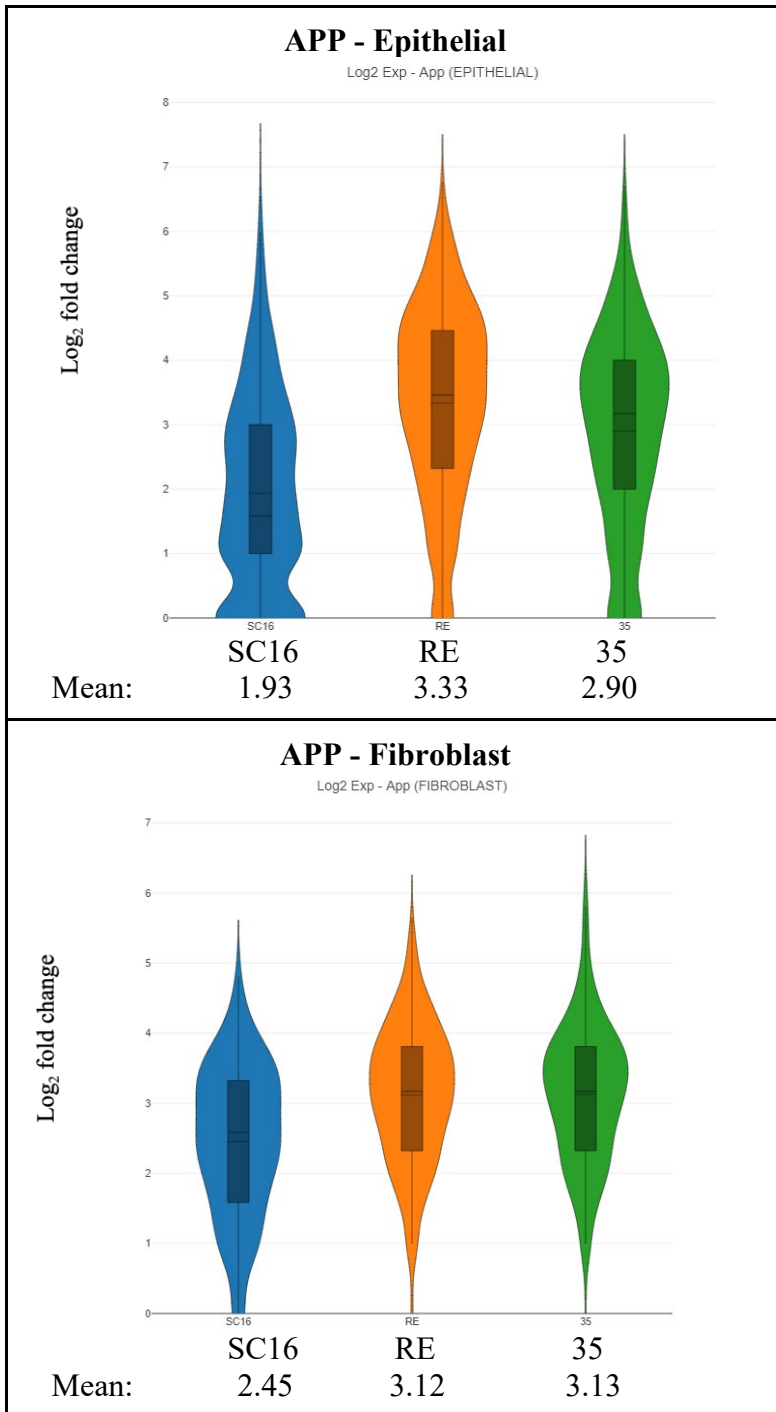
Figure 7. Violin Plots of Epithelial and Fibroblast Expression of APP using Loupe GEX Browser. Epithelial cells (Top) were identified by expression of KRT12. Fibroblast cells (Bottom) were identified by expression of FBN-1.
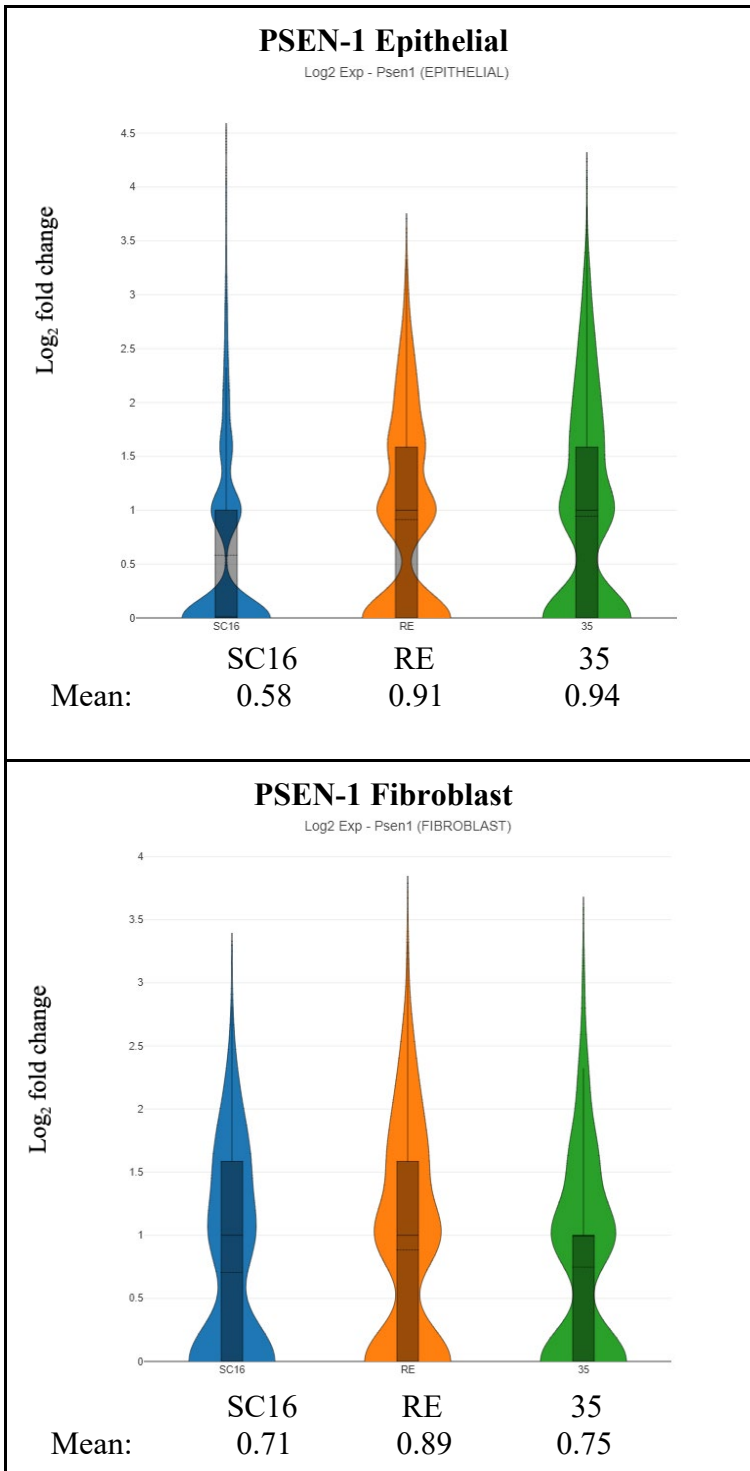
Figure 8. Violin Plots of Epithelial and Fibroblast Expression of PSEN-1 using Loupe GEX Browser. Epithelial cells (Top) were identified by expression of KRT12. Fibroblast cells (Bottom) were identified by expression of FBN-1.
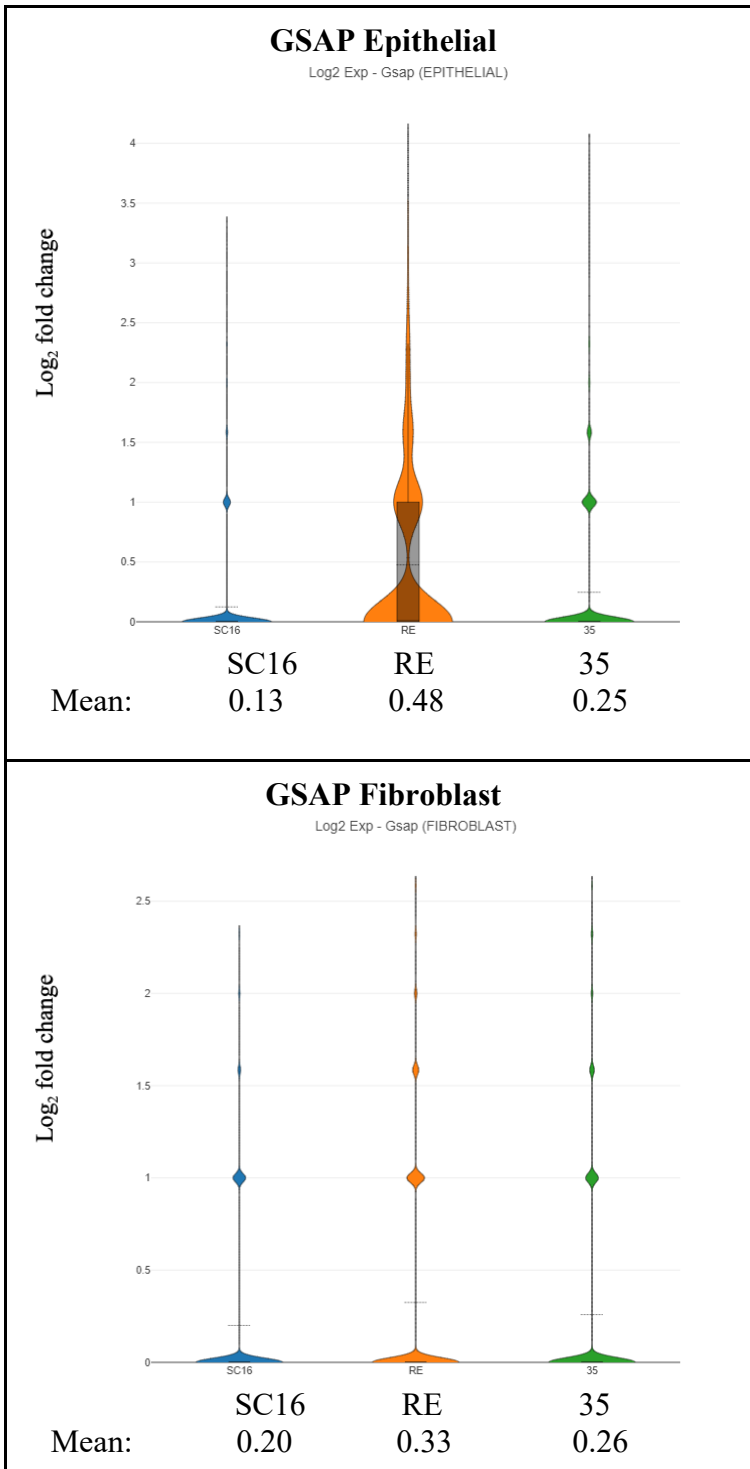
Figure 9. Violin Plots of Epithelial and Fibroblast Expression of GSAP using Loupe GEX Browser. Epithelial cells (Top) were identified by expression of KRT12. Fibroblast cells (Bottom) were identified by expression of FBN-1.

Table 3. 10X Relative Gene Expression Summary for Epithelial Cells.

Epithelial Cells		HSV-1 Strain		
		SC16	**RE**	**35**
Gene Expression (— lowest, ↑ medial, ↑↑ highest)	**APP**	— 1.9	↑↑ 3.3	↑ 2.9
	PSEN-1	— 0.58	↑ 0.91	↑ 0.94
	GSAP	— 0.13	↑↑ 0.48	↑ 0.25

Table 4. 10X Relative Gene Expression Summary for Fibroblasts.

Fibroblasts		HSV-1 Strain		
		SC16	**RE**	**35**
Gene Expression (— lowest, ↑ medial, ↑↑ highest)	**APP**	— 2.5	↑ 3.1	↑ 3.1
	PSEN-1	— 0.71	↑↑ 0.89	— 0.75
	GSAP	— 0.20	↑↑ 0.33	— 0.26

Figure 10. Violin Plots of Epithelial and Fibroblast Expression of BACE-1 using Loupe GEX Browser. Epithelial cells (Top) were identified by expression of KRT12. Fibroblast cells (Bottom) were identified by expression of FBN-1. Mock conditions signify infected media.
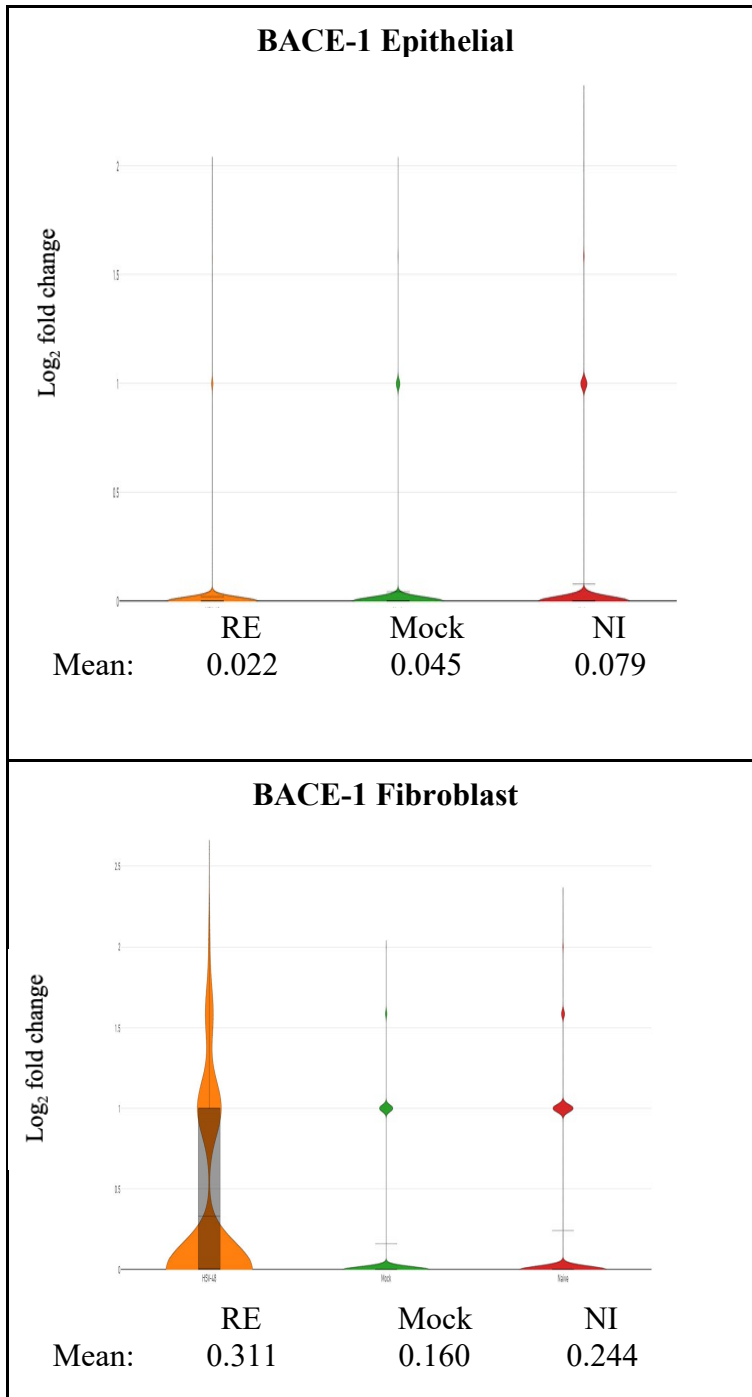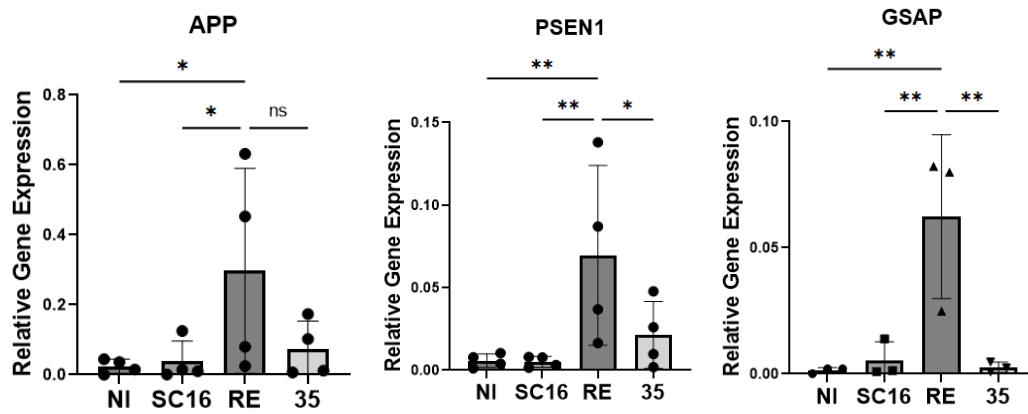
Figure 11. Relative Gene Expression via RT-qPCR. Relative gene expression of APP (left), PSEN-1 (middle), and GSAP (right) in NI, SC16-, RE-, and 35-infected murine corneal fibroblasts via RT-qPCR. Symbols indicate the mean value of a single RT-qPCR analysis. * $p<0.04$, ** $p<0.009$. One-Way ANOVA with Tukey's multiple comparisons.
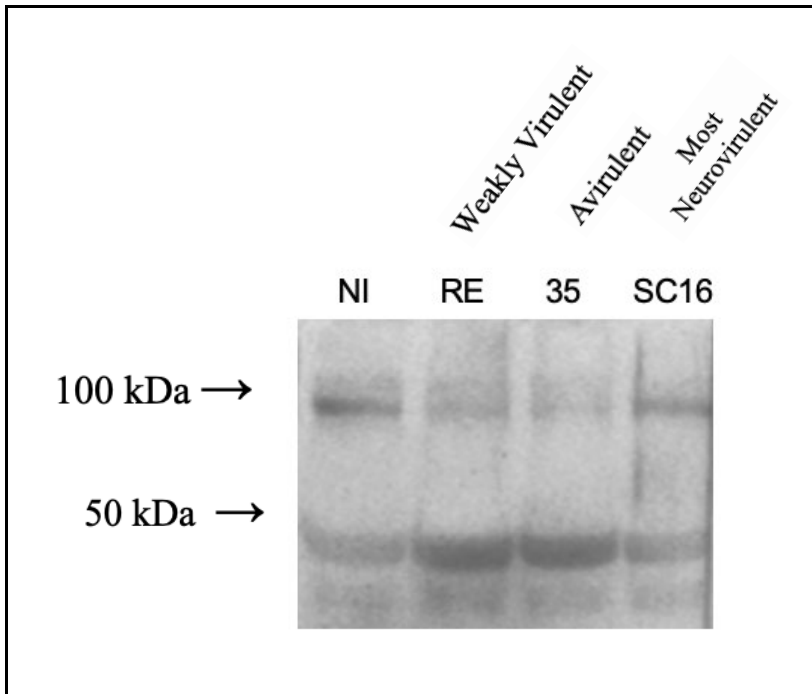
Figure 12. APP Levels via Western Blot. Western blot of supernatants from corneal fibroblasts detecting Aβ ~45 kDa and sAPPα ~100 kDa (M3.2 monoclonal antibody).
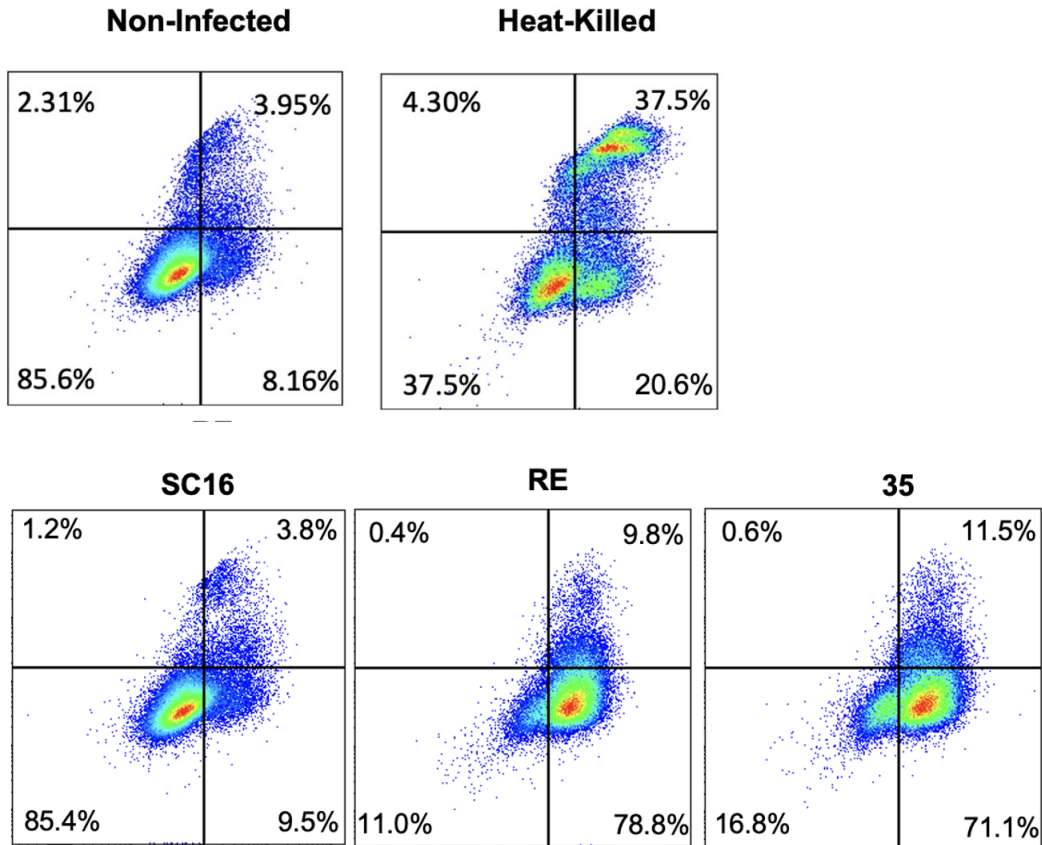
Figure 13. Cell Death Assay. Flow cytometric analysis of non-infected (top left, negative control), heat treated (top right, positive control), and HSV-1 infected fibroblasts using Annexin V and PI 48 hours post-infection of SC16 (bottom left), RE (bottom middle), 35 (bottom right).
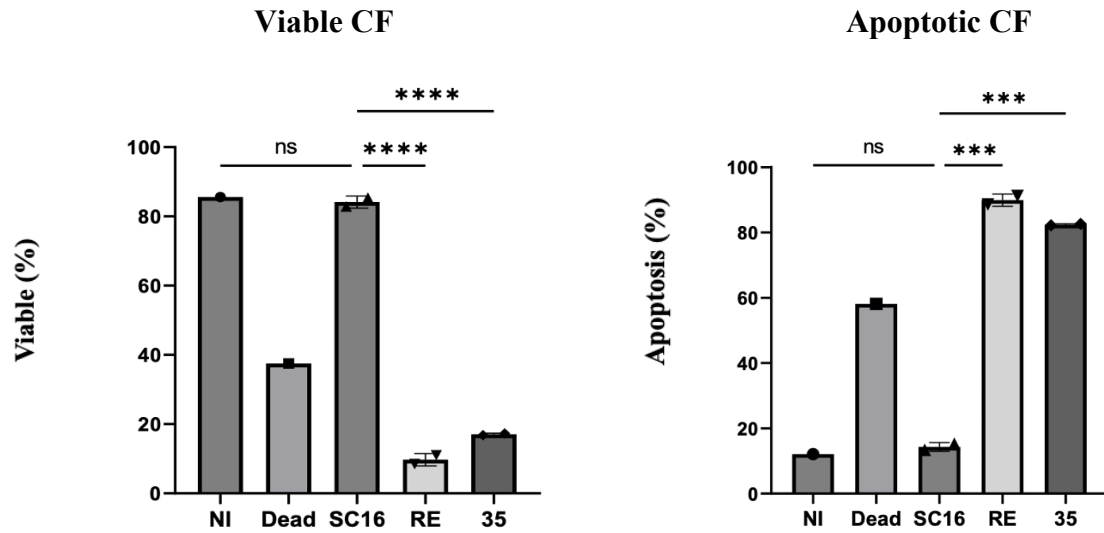
Figure 14. Cell Death Comparison Plots. Frequency of viable (left) and apoptotic (right) cells following 48 hour infection with SC16, RE, or 35. Each symbol indicates mean percentage of a single flow cytometric analysis. Data shown summarize two independent experiments. *** $p<0.006$, **** $p<0.001$. Two-Way ANOVA with Tukey's multiple comparisons.
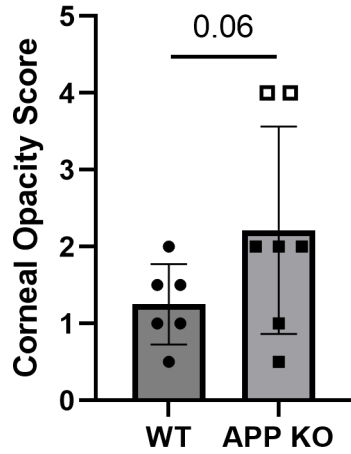
Figure 15. Quantification of Opacity Scores in Corneas of HSV-1 RE Infected Mice.

Corneal opacity scores were determined by blinded corneal opacity scores using corneas from WT (circles) and APP KO (squares) mice 48-hours post-infection. Each symbol represents data from a single cornea; filled symbols were from male mice, open symbols were from female mice. Bars indicate standard deviation, One-Tailed Mann-Whitney Test; *p*-value approaching significance is shown on plot.
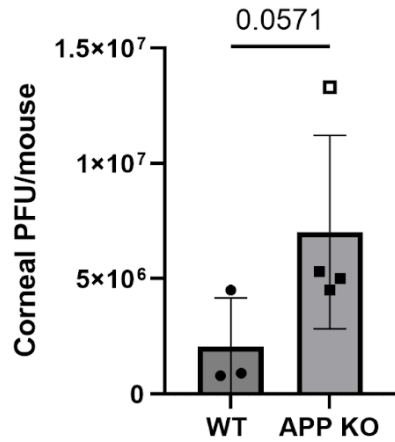
Figure 16. Quantitation of HSV-1 RE in Corneas of Infected Mice. PFU were determined by Plaque Assay using corneas from WT (circles) and APP KO (squares) mice 48-hours post-infection. Each symbol represents data from a single cornea; filled symbols were from male mice, open symbols were from female mice. Bars indicate standard deviation, One-Tailed Mann-Whitney Test; *p*-value = 0.0571.
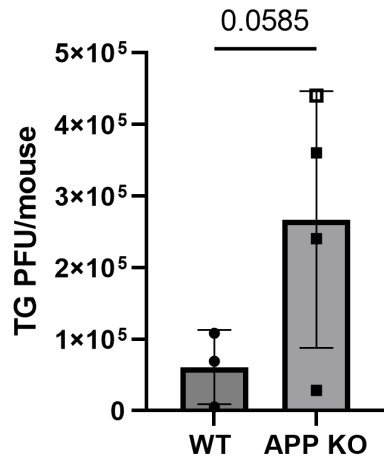
Figure 17. Quantification of HSV-1 RE in Trigeminal Ganglia (TG) of Infected Mice.

TG PFU were determined by Plaque Assay using TG from WT (circles) and APP KO (squares) mice 48-hours post-infection. Each symbol represents data from a single TG; filled symbols were from male mice, open symbols were from female mice. Bars indicate standard deviation, One-Tailed Unpaired T-test; p-value $= 0.0585$.
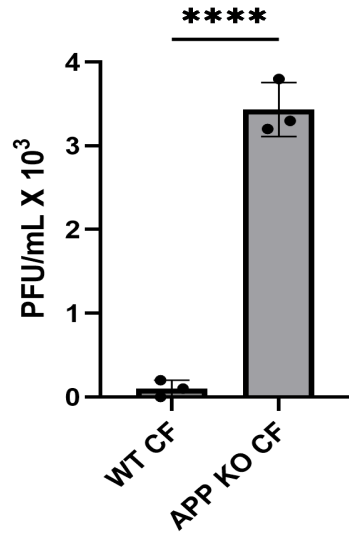
Figure 18. Quantitation of HSV-1 SC16 in Corneal Fibroblasts. PFU were determined

by Plaque Assay using WT and APP KO corneal fibroblasts 24-hours post-infection.

Each symbol represents data from a single sample. Bars indicate standard deviation,

unpaired T-test; *** *p*<0.0001.
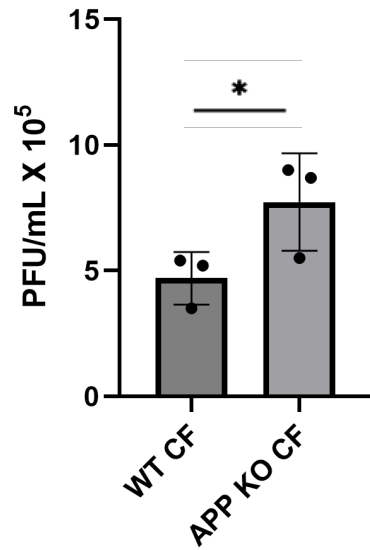
Figure 19. Quantitation of HSV-1 RE in Corneal Fibroblasts. PFU were determined by Plaque Assay using WT and APP KO corneal fibroblasts 24-hours post-infection. Each symbol represents data from a single sample. Bars indicate standard deviation, unpaired T-test, * p-value = 0.0378.
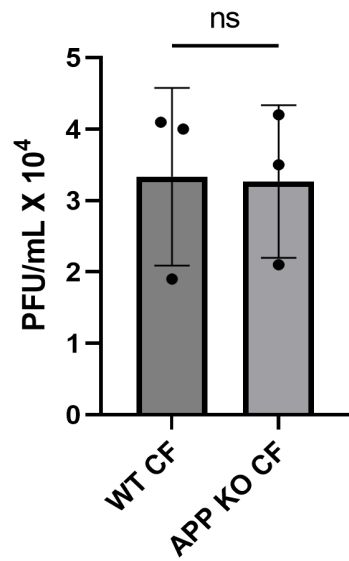
Figure 20. Quantitation of HSV-1 35 in Corneal Fibroblasts. PFU were determined by

Plaque Assay using WT and APP KO corneal fibroblasts 24-hours post-infection. Each

symbol represents data from a single sample. Bars indicate standard deviation, unpaired

T-test.

CHAPTER V

DISCUSSION

5.1 Relative Gene Expression

The corneas of mice were subjected to infection with HSV-1 strains SC16, RE, and 35, followed by processing through the 10X genomics workflow. Analysis of single-cell RNA sequencing data revealed that epithelial cells and fibroblasts infected with HSV-1 SC16 had diminished observable expression of APP, PSEN-1, and GSAP compared to those infected with RE and 35. We propose that the different strains of HSV-1 may vary in their tropism, thus inducing APP, PSEN-1, and GSAP differentially within corneas of mice. For example, the most neurovirulent strain used, SC16, may have a higher tropism for neurons and thus infect fewer epithelial cells and fibroblasts in comparison to RE and 35. Future studies will incorporate reference genomes for each HSV-1 strain into the compiled scRNAseq libraries to allow us to address this hypothesis.

Notably, expression of PSEN-1 was observed in NI corneas of mice as well as NI corneal fibroblasts *in vitro.* Presenilin-1, the product of PSEN-1, is involved in both the amyloidogenic and non-amyloidogenic pathways, potentially explaining why constitutive expression of PSEN-1 is observed. As shown in **Table 3**, PSEN-1 transcript abundance was similar in corneas infected with RE and 35 in epithelial cells (0.04 Log_2Fold difference). Similarly, differences in transcript abundance of PSEN-1 were larger within

fibroblasts from corneas infected with RE and 35 (0.14 Log$_2$Fold difference) as shown in

Table 4. In both cell types, SC16 infection resulted in the lowest relative gene

expression. However, in fibroblasts, SC16 was not observably greatly different from 35

(0.04 Log$_2$Fold difference), possibly due to greater tropism for certain cell

types. Relative transcript levels of PSEN-1 via RT-qPCR *in vitro* of corneal fibroblasts

infected with SC16, RE, or 35 were consistent with *in vivo* gene expression of fibroblasts.

RT-qPCR data showed RE infection caused significant elevation of PSEN-1 compared to

both SC16 (*p*<0.009) and 35 (*p*<0.004). Likewise, PSEN-1 expression was elevated in

RE in fibroblasts *in vivo*. Furthermore, SC16 and 35 infections were not statistically

significant in corneal fibroblasts *in vitro*, similar to what was observed in fibroblasts *in*

vivo (0.04 Log$_2$Fold difference). This, further suggests a greater proclivity of SC16

infection in nervous tissue as SC16-infected mice have a greater and faster mortality rate

than RE and 35 infected mice. Differences in PSEN-1 expression both *in vivo* and *in vitro*

implicate differential cleavage responses among the three HSV-1 strains. Presenilin-1 is

involved in the cleavage of several other type-I transmembrane proteins and therefore

PSEN-1 may expressed in NI and infected fibroblasts through differing mechanisms (De

Strooper *et al*., 2012). Our lab addressed whether HSV-1 may promote PSEN-1

transcription *in vitro.* We found a significant difference between RE infected and NI

fibroblasts suggesting that certain HSV-1 strains may heighten transcription of PSEN-1

in the cell. To validate HSV-1 induced PSEN-1 expression in fibroblasts, further

investigation *in vivo* comparing the expression of PSEN-1 in infected conditions to NI

cells is needed.

The gene encoding for ɣ-secretase activating protein, GSAP, is also part of the ɣ-secretase complex. *In vivo,* GSAP expression in fibroblasts was elevated in RE in comparison to SC16 and 35. However, SC16 was not greatly different from 35 (0.06 Log$_2$Fold difference) in fibroblasts *in vivo*. *In vitro* data found RE infected cells had significantly greater GSAP expression levels in comparison to SC16, 35, and NI conditions, while SC16 and 35 infections were not different, which is similar to the observed *in vivo* expression. Similarly, epithelial cells expressing GSAP *in vivo* had the lowest expression in SC16 infection, while RE was the greatest (0.35 Log$_2$Fold difference). Differences in the expression of GSAP between epithelial and fibroblasts from SC16 infected corneas show there is variance across cell types. These variations may be due to differences in cell infectivity, viral replication cycles, or the cell's ability to go through the amyloidogenic pathway.

In the amyloidogenic pathway, the initial cleavage of APP through β-secretase generates soluble amyloid precursor protein beta (sAPPβ). Secondary cleavage by ɣ-secretase, consisting of the proteins encoded by PSEN-1 and GSAP genes, creates smaller Aβ peptides. Average β-secretase expression *in vivo* was increased in RE infected fibroblasts in comparison to both NI and mock conditions. Contrastingly, there was less β-secretase expression in RE infected epithelial cells compared to NI and mock conditions *in vivo*. Increased β-secretase expression in RE infected fibroblasts may suggest an increased mediation of the amyloidogenic pathway, while lower β-secretase expression in RE infected epithelial cells suggests a greater preference for the normal, non-amyloidogenic pathway.

5.2 Protein Levels

Western blot analyses were conducted using supernatants obtained from HSV-1-infected fibroblast cells. Supernatants of both NI cells and those infected with SC16 had elevated levels of sAPPα (~100 kDa), a peptide cleaved irreversibly upon stimulation into the non-amyloidogenic pathway, compared to more processed non-soluble APP peptides produced from the amyloidogenic pathway (~45 kDa), which we posit as Aβ peptides. In contrast, cells infected with RE and 35 displayed a higher abundance of fully processed APP relative to larger soluble APP. These findings may imply that RE and 35 strains induced the amyloidogenic pathway to produce Aβ (~45 kDa). Furthermore, increased cleaved peptide production from HSV-1 infected RE and 35 strains in comparison to NI cells indicate the heightened amyloid-producing response of HSV-1 infection.

Additionally, an observable band corresponding to Aβ (~45 kDa) in all conditions indicates that both NI and SC16 HSV-1 infected cells may go through the amyloidogenic pathway. Under physiological conditions, APP is preferably metabolized by the non-amyloidogenic pathway which is comparable to our data exemplifying a greater band density of sAPPα in NI conditions (de Paula *et al.,* 2009). However, the presence of a band ~45 kDa in both NI and SC16 could indicate the activation of the underlying stress-inducing pathways, cell death-associated release of the peptides, or a combination thereof.

5.3 Cell Death Assay

A flow cytometry-based cell death assay served as a metric for the infectivity of corneal fibroblasts as HSV-1 infected cells typically undergo apoptosis. Levels of viable SC16 infected *in vitro* corneal fibroblasts were not significantly different from NI cells,

potentially attributable to their diminished infectivity in fibroblasts and heightened affinity towards neurons. In contrast, RE and 35 infected cells were significantly different than SC16, displaying a greater apoptotic response.

Plaque assay 24 hours post-infection of HSV-1 SC16, RE, and 35 in WT corneal fibroblasts showed the greatest viral titer in RE infected fibroblasts which is consistent with our cell death assay. SC16 infected fibroblasts showed the lowest viral titer which is consistent with our experimental hypothesis of greater tropism for neurons. Corneal fibroblasts infected with HSV-1 35 had low viral titer, which differs from our flow cytometry data of HSV-1 35 infection 48-hour post infection. As a type-1 interferon sensitive strain, our data suggests that HSV-1 35 may successfully infect fibroblasts, however, trigger an immune response during initial infection preventing viral replication.

5.4 Neutralization of HSV-1

The APP KO mice had greater average corneal opacity from RE infection compared to that observed in WT mice, suggesting that APP can limit HSV-1 infection and/or replication. Viral burden of cornea infect with RE was not increased in the absence of APP which may be due to other immune or inflammatory responses in whole cornea samples. Given that HSV-1 can establish latency in the trigeminal ganglia, the higher viral titers in the TG of APP KO mice suggest that APP limits the spread of HSV-1.

Plaque assay *in vitro* found a significant increase in viral burden in SC16 and RE infected APP KO fibroblasts in comparison to WT fibroblasts which suggest an immunoprotective role of APP in corneal fibroblasts infected with HSV-1. Greater

abundance of Aβ observed in the western blot and lower viral titer of RE infected WT CF compared to RE infected APP KO CF are consistent with the antiviral hypothesis. Lower viral titer in SC16 infection in APP WT fibroblasts and a greater abundance of soluble sAPPα observed via the western blot is consistent with previous data suggesting non-amyloidogenic sAPPα promotes neuronal survival (Hefter *et al.,* 2017). However, whether varying viral titers of SC16 or RE infected APP KO and WT corneal fibroblasts are due to differences in infectivity and/or replication is unclear. Similar viral titers between HSV-1 35 APP KO and WT fibroblasts is consistent with the idea that initial infection triggers a different protective immune response not dependent on APP. Differences between viral titer across HSV-1 SC16, RE, and 35 infected APP KO and WT fibroblasts *in vitro* suggest that HSV-1 neutralization may be dependent on virulence.

CHAPTER VI

CONCLUSIONS

Every year in the United States, there are over 3 million cases of AD, characterized by the presence of Aβ plaques. Infection with neurotropic HSV-1 can lead to lifelong repeated activation, ultimately triggering protective immune pathways. The role of APP and Aβ, during HSV-1 infection is not well defined. Therefore, it is unclear whether 1) APP and/or Aβ is protective against HSV-1 infection and spread, and/or 2) whether HSV-1 infection potentiates the development of AD. Experiments described herein addressed whether APP production and processing differed following infection with three different strains of HSV-1 that varied in their neurovirulence.

We found that the most neurovirulent strain induced less APP expression and production in comparison to the moderately and weakly virulent strains. Interestingly, we noted lower expression of APP, PSEN-1, and GSAP in corneal fibroblasts and epithelial cells from SC16 infected mice compared to those in RE and 35 infected mice. In combination, with SC16 causing greater mortality *in vivo* suggests to us that SC16 has a greater tropism for neurons, and infects fewer corneal fibroblasts and epithelial cells. In sum, our studies support that APP production and processing is differential across HSV-1 strains due to differences in the proteins' role upon infection with a specific strain.

46

While direct testing of the role of APP in shaping the neurovirulence of HSV-1 wasn't conducted, our data strongly indicates its involvement. We observed higher expression and production of APP following HSV-1 RE infection compared to SC16, both *in vivo* and *in vitro*. This suggests that moderately virulent strains may generate higher levels of APP than their more neurovirulent counterparts, supporting the notion of APP's influence on neurovirulence.

Our data suggests that APP is produced as part of an innate immune response against HSV-1 as APP KO mice and fibroblasts showed greater viral burden than WT mice and fibroblasts. Our data also suggest APP plays a role in viral spread to the TG that would conceivably extend to the brain, though we need to test this directly. APP production as part of the immune response may not be necessary for less virulent strains such as HSV-1 35, as 35 is known to be sensitive to other immune pathways such as the production of type-1 interferon.

In a broader context, these findings may imply that distinct strains of the virus can result in varied clinical manifestations or outcomes. Low SC16 infection and/or replication in corneal cells, accompanied with high mortality suggest a fast viral spread directly to the brain. Applying this reasoning, it follows that individuals infected with more neurovirulent strains are at a higher risk of mortality from herpes simplex encephalitis (HSE). In contrast, weakly virulent strains would be limited to inducing ocular manifestations as they do not spread as readily to the brain. The moderately neurovirulent strains would then be the most problematic as these would be able to enter the TG and brain upon initial infection but be less lethal and therefore, likely stay in a latent phase. Thus, moderately virulent strains may be more prone to reactivation and

therefore may increase both ocular pathology as well as infection in the brain leading to increased production of APP in neurons likely causing or contributing to AD pathogenesis and/or progression. However, the idea that neurons are able to induce APP production from HSV-1 strains is unknown and would require experiments using brain tissue, similar to those presented herein for cornea. Additionally, whether increased or decreased processing and/or production of APP is limited to HSV-1 infected cells or is part of an indirect immune response is also unknown. *In vivo* confirmation of HSV-1 infection across the samples is crucial to determine whether differences are due to cell infectivity or replication cycles of the strain.

In conclusion, these observations highlight the potential significance of strain-specific differences in HSV-1 infection, suggesting varying clinical outcomes based on neurovirulence. Further exploration, particularly within the brain, is essential to elucidate the mechanisms underlying these findings and their implications for both ocular pathology and central nervous system infection.

REFERENCES

Agostini, Simone, Roberta Mancuso, Francesca Baglio, Monia Cabinio, Ambra Hernis, Franca
   Rosa Guerini, Elena Calabrese, Raffaello Nemni, and Mario Clerici. "Lack of Evidence
   for a Role of HHV-6 in the Pathogenesis of Alzheimer's Disease." Edited by Marco
   Bozzali. *Journal of Alzheimer's Disease* 49, no. 1 (November 3, 2015): 229–35.
   https://doi.org/10.3233/JAD-150464.

Alonso-Vanegas, Mario Arturo, Eduardo Quintero-López, Adrián Axallacan Martínez-
   Albarrán, and Juan Carlos Moreira-Holguín. "Recurrent Herpes Simplex Virus
   Encephalitis After Neurologic Surgery." *World Neurosurgery* 89 (May 2016): 731.e1-
   731.e5. https://doi.org/10.1016/j.wneu.2016.01.057.

Ball, Melvyn J. "Limbic Predilection in Alzheimer Dementia: Is Reactivated Herpesvirus
   Involved?" *Canadian Journal of Neurological Sciences / Journal Canadien Des Sciences
   Neurologiques* 9, no. 3 (August 1982): 303–6.
   https://doi.org/10.1017/S0317167100044115.

Bocharova, Olga, Narayan P. Pandit, Kara Molesworth, Aidan Fisher, Olga Mychko, Natallia
   Makarava, and Ilia V. Baskakov. "Alzheimer's Disease-Associated β-Amyloid Does Not
   Protect against Herpes Simplex Virus 1 Infection in the Mouse Brain." *Journal of*

Biological Chemistry 297, no. 1 (July 2021): 100845.

https://doi.org/10.1016/j.jbc.2021.100845.

Cairns, Dana M., Nicolas Rouleau, Rachael N. Parker, Katherine G. Walsh, Lee Gehrke, and

David L. Kaplan. "A 3D Human Brain-like Tissue Model of Herpes-Induced Alzheimer's

Disease." *Science Advances* 6, no. 19 (May 2020): eaay8828.

https://doi.org/10.1126/sciadv.aay8828.

Chu, Hiutung, Marzena Pazgier, Grace Jung, Sean-Paul Nuccio, Patricia A. Castillo, Maarten

F. De Jong, Maria G. Winter, et al. "Human α-Defensin 6 Promotes Mucosal Innate

Immunity Through Self-Assembled Peptide Nanonets." *Science* 337, no. 6093 (July 27,

2012): 477–81. https://doi.org/10.1126/science.1218831.

Conrady, Christopher D., Douglas A. Drevets, and Daniel J.J. Carr. "Herpes Simplex Type I

(HSV-1) Infection of the Nervous System: Is an Immune Response a Good Thing?"

Journal of Neuroimmunology 220, no. 1–2 (March 2010): 1–9.

https://doi.org/10.1016/j.jneuroim.2009.09.013.

De Strooper, Bart, Takeshi Iwatsubo, and Michael S. Wolfe. "Presenilins and γ-Secretase:

Structure, Function, and Role in Alzheimer Disease." *Cold Spring Harbor Perspectives*

in Medicine 2, no. 1 (January 2012): a006304.

https://doi.org/10.1101/cshperspect.a006304.

Eimer, William A., Deepak Kumar Vijaya Kumar, Nanda Kumar Navalpur Shanmugam, Alex

S. Rodriguez, Teryn Mitchell, Kevin J. Washicosky, Bence György, Xandra O.

Breakefield, Rudolph E. Tanzi, and Robert D. Moir. "Alzheimer's Disease-Associated β-

Amyloid Is Rapidly Seeded by Herpesviridae to Protect against Brain Infection." *Neuron*

99, no. 1 (July 2018): 56-63.e3. https://doi.org/10.1016/j.neuron.2018.06.030.

Farooq, Asim V., and Deepak Shukla. "Herpes Simplex Epithelial and Stromal Keratitis: An Epidemiologic Update." *Survey of Ophthalmology* 57, no. 5 (September 2012): 448–62. https://doi.org/10.1016/j.survophthal.2012.01.005.

Fenton, Robin R., Sara Molesworth-Kenyon, John E. Oakes, and Robert N. Lausch. "Linkage of IL-6 with Neutrophil Chemoattractant Expression in Virus-Induced Ocular Inflammation." *Investigative Ophthalmology & Visual Science* 43, no. 3 (March 2002): 737–43.

Hefter, Dimitri, and Andreas Draguhn. "APP as a Protective Factor in Acute Neuronal Insults." *Frontiers in Molecular Neuroscience* 10 (February 2, 2017). https://doi.org/10.3389/fnmol.2017.00022.

Hill, T. J., H. J. Field, and W. A. Blyth. "Acute and Recurrent Infection with Herpes Simplex Virus in the Mouse: A Model for Studying Latency and Recurrent Disease." *The Journal of General Virology* 28, no. 3 (September 1975): 341–53. https://doi.org/10.1099/0022-1317-28-3-341.

Itzhaki, Ruth F. "Herpes Simplex Virus Type 1 and Alzheimer's Disease: Possible Mechanisms and Signposts." *The FASEB Journal* 31, no. 8 (August 2017): 3216–26. https://doi.org/10.1096/fj.201700360.

Jeong, Hyun-Hwan, and Zhandong Liu. "Are HHV-6A and HHV-7 Really More Abundant in Alzheimer's Disease?" *Neuron* 104, no. 6 (December 2019): 1034–35. https://doi.org/10.1016/j.neuron.2019.11.009.

Knotts, F. B., M. L. Cook, and J. G. Stevens. "Pathogenesis of Herpetic Encephalitis in Mice after Ophthalmic Inoculation." *Journal of Infectious Diseases* 130, no. 1 (July 1, 1974): 16–27. https://doi.org/10.1093/infdis/130.1.16.

Kumar, Anil, Jaskirat Sidhu, Amandeep Goyal, and Jack W. Tsao. "Alzheimer Disease." In
    StatPearls. Treasure Island (FL): StatPearls Publishing, 2023.
    http://www.ncbi.nlm.nih.gov/books/NBK499922/.

Kumar, Deepak Kumar Vijaya, Se Hoon Choi, Kevin J. Washicosky, William A. Eimer,
    Stephanie Tucker, Jessica Ghofrani, Aaron Lefkowitz, et al. "Amyloid-β Peptide Protects
    against Microbial Infection in Mouse and Worm Models of Alzheimer's Disease."
    Science Translational Medicine 8, no. 340 (May 25, 2016): 340ra72.
    https://doi.org/10.1126/scitranslmed.aaf1059.

Looker, Katharine J., Amalia S. Magaret, Margaret T. May, Katherine M. E. Turner, Peter
    Vickerman, Sami L. Gottlieb, and Lori M. Newman. "Global and Regional Estimates of
    Prevalent and Incident Herpes Simplex Virus Type 1 Infections in 2012." Edited by Neal
    A. DeLuca. *PLOS ONE* 10, no. 10 (October 28, 2015): e0140765.
    https://doi.org/10.1371/journal.pone.0140765.

Marcocci, Maria Elena, Giorgia Napoletani, Virginia Protto, Olga Kolesova, Roberto
    Piacentini, Domenica Donatella Li Puma, Patrick Lomonte, Claudio Grassi, Anna Teresa
    Palamara, and Giovanna De Chiara. "Herpes Simplex Virus-1 in the Brain: The Dark
    Side of a Sneaky Infection." *Trends in Microbiology* 28, no. 10 (October 2020): 808–20.
    https://doi.org/10.1016/j.tim.2020.03.003.

Metcalf, J. F., and B. A. Michaelis. "Herpetic Keratitis in Inbred Mice." *Investigative
    Ophthalmology & Visual Science* 25, no. 10 (October 1984): 1222–25.

Murphy, M. Paul, and Harry LeVine. "Alzheimer's Disease and the Amyloid-β Peptide."
    Edited by Mark A. Lovell. *Journal of Alzheimer's Disease* 19, no. 1 (January 6, 2010):
    311–23. https://doi.org/10.3233/JAD-2010-1221.

Noble, James E., and Marc J.A. Bailey. "Chapter 8 Quantitation of Protein." In *Methods in Enzymology*, 463:73–95. Elsevier, 2009. https://doi.org/10.1016/S0076-6879(09)63008-1.

Paula, Vanessa de Jesus R. de, Fabiana Meira Guimarães, Breno Satler Diniz, and Orestes Vicente Forlenza. "Neurobiological Pathways to Alzheimer's Disease: Amyloid-Beta, TAU Protein or Both?" *Dementia & Neuropsychologia* 3, no. 3 (2009): 188–94. https://doi.org/10.1590/S1980-57642009DN30300003.

Rajcáni, J., U. Herget, and H. C. Kaerner. "Spread of Herpes Simplex Virus (HSV) Strains SC16, ANG, ANGpath and Its glyC Minus and GlyE Minus Mutants in DBA-2 Mice." *Acta Virologica* 34, no. 4 (August 1990): 305–20.

Readhead, Ben, Jean-Vianney Haure-Mirande, Cory C. Funk, Matthew A. Richards, Paul Shannon, Vahram Haroutunian, Mary Sano, et al. "Multiscale Analysis of Independent Alzheimer's Cohorts Finds Disruption of Molecular, Genetic, and Clinical Networks by Human Herpesvirus." *Neuron* 99, no. 1 (July 11, 2018): 64-82.e7. https://doi.org/10.1016/j.neuron.2018.05.023.

Roizman, Bernard, and Guoying Zhou. "The 3 Facets of Regulation of Herpes Simplex Virus Gene Expression: A Critical Inquiry." *Virology* 479–480 (May 2015): 562–67. https://doi.org/10.1016/j.virol.2015.02.036.

Sanders, Rebecca, Deborah J. Mason, Carole A. Foy, and Jim F. Huggett. "Considerations for Accurate Gene Expression Measurement by Reverse Transcription Quantitative PCR When Analysing Clinical Samples." *Analytical and Bioanalytical Chemistry* 406, no. 26 (October 2014): 6471–83. https://doi.org/10.1007/s00216-014-7857-x.

Schmoldt, A., H. F. Benthe, and G. Haberland. "Digitoxin Metabolism by Rat Liver Microsomes." *Biochemical Pharmacology* 24, no. 17 (September 1, 1975): 1639–41.

Smiley, M. L., J. A. Hoxie, and H. M. Friedman. "Herpes Simplex Virus Type 1 Infection of Endothelial, Epithelial, and Fibroblast Cells Induces a Receptor for C3b." *Journal of Immunology (Baltimore, Md.: 1950)* 134, no. 4 (April 1985): 2673–78.

Soscia, Stephanie J., James E. Kirby, Kevin J. Washicosky, Stephanie M. Tucker, Martin Ingelsson, Bradley Hyman, Mark A. Burton, et al. "The Alzheimer's Disease-Associated Amyloid β-Protein Is an Antimicrobial Peptide." Edited by Ashley I. Bush. *PLoS ONE* 5, no. 3 (March 3, 2010): e9505. https://doi.org/10.1371/journal.pone.0009505.

Su, Y. H., J. E. Oakes, and R. N. Lausch. "Ocular Avirulence of a Herpes Simplex Virus Type 1 Strain Is Associated with Heightened Sensitivity to Alpha/Beta Interferon." *Journal of Virology* 64, no. 5 (May 1990): 2187–92. https://doi.org/10.1128/JVI.64.5.2187-2192.1990.

Su, Y.-H., J. E. Oakes, and R. N. Lausch. "Mapping the Genetic Region Coding for Herpes Simplex Virus Resistance to Mouse Interferon /Beta." *Journal of General Virology* 74, no. 11 (November 1, 1993): 2325–32. https://doi.org/10.1099/0022-1317-74-11-2325.

Torrent, Marc, David Pulido, M. Victòria Nogués, and Ester Boix. "Exploring New Biological Functions of Amyloids: Bacteria Cell Agglutination Mediated by Host Protein Aggregation." Edited by H. Steven Seifert. *PLoS Pathogens* 8, no. 11 (November 1, 2012): e1003005. https://doi.org/10.1371/journal.ppat.1003005.

Westman, Gabriel, Jonas Blomberg, Zhibing Yun, Lars Lannfelt, Martin Ingelsson, and Britt-Marie Eriksson. "Decreased HHV-6 IgG in Alzheimer's Disease." *Frontiers in Neurology* 8 (February 20, 2017). https://doi.org/10.3389/fneur.2017.00040.

Whitson, Heather E., Carol Colton, Joseph El Khoury, David Gate, Alison Goate, Michael T. Heneka, Rima Kaddurah-Daouk, et al. "Infection and Inflammation: New Perspectives on Alzheimer's Disease." *Brain, Behavior, & Immunity - Health* 22 (July 2022): 100462. https://doi.org/10.1016/j.bbih.2022.100462.

Yang, Ping-Chang, and Tahrin Mahmood. "Western Blot: Technique, Theory, and Trouble Shooting." *North American Journal of Medical Sciences* 4, no. 9 (2012): 429. https://doi.org/10.4103/1947-2714.100998.

BIOGRAPHICAL SKETCH

Name of Author: Mia Elias

Undergraduate Schools Attended: University of South Alabama

Degrees Awarded: B. S. in Biomedical Sciences, Anticipated May 2024

Awards and Honors:

University of South Alabama Honors College

2020-2024 Talent Tier 5 South Alabama Scholarship Recipient

2023 Summer Undergraduate Research Fellowship Recipient

2023 Undergraduate Research Symposium Speaker

2024 National Conference of Undergraduate Research Speaker

Mortar Board National Honor Society Treasurer

Alpha Epsilon Delta Medical Honor Society

Chi Omega Phi Sigma Iota Foreign Language Society

Women's Pre-Health Club